THE HARD X-RAY TELESCOPE (HXT) FOR THE SOLAR-A MISSION*

T. KOSUGI[1], K. MAKISHIMA[2], T. MURAKAMI[3], T. SAKAO[4], T. DOTANI[3], M. INDA[2], K. KAI[4], S. MASUDA[1], H. NAKAJIMA[4], Y. OGAWARA[3], M. SAWA[4], and K. SHIBASAKI[4]

(Received 22 March, 1991; in revised form 27 May, 1991)

Abstract. The Hard X-ray Telescope (HXT) is a Fourier-synthesis imager; a set of spatially-modulated photon count data are taken from 64 independent subcollimators and are Fourier-transformed into an image by using procedures such as the maximum entropy method (MEM) or CLEAN. The HXT takes images of solar flares simultaneously in four energy bands, nominally 15 (or 19)–24, 24–35, 35–57, and 57–100 keV, with an ultimate angular resolution as fine as ~ 5 arc sec and a time resolution 0.5 s. Each subcollimator has a field of view wider than the solar disk. The total effective area of the collimator/detector system reaches ~ 70 cm^2, about one order of magnitude larger than that of the HINOTORI hard X-ray imager. Thanks to these improvements, HXT will for the first time enable us to take images of flares at photon energies above ~ 30 keV. These higher-energy images will be compared with lower-energy ones, giving clues to the understanding of nonthermal processes in solar flares, i.e., the acceleration and confinement of energetic electrons. It is of particular importance to specify the acceleration site with regard to the magnetic field figuration in a flaring region, which will be achieved by collaborative observations between HXT and the Soft X-ray Telescope on board the same mission.

1. Introduction

The SOLAR-A mission is the second satellite of the Institute of Space and Astronautical Science, Japan (ISAS) dedicated to the study of solar flares. The first solar-flare mission, HINOTORI, was launched during the previous maximum in February 1981. At that time the Solar Maximum Mission (SMM) had been in operation for about one year with almost the same scientific objectives as HINOTORI. Each of the two missions conducted a wide variety of observations in the X- and γ-ray ranges (including EUV and visible-light observations in the case of SMM), and diagnosed high-energy particles and high-temperature plasmas involved in flares. In particular, the two missions made the first hard X-ray imaging observations of flares (Van Beek *et al.*, 1980; Makishima, 1982).

Hard X-rays are produced by collisions of high-energy electrons with ions (bremsstrahlung) and their propagation is almost unaffected by the solar atmosphere above the photosphere. Accordingly, images taken in this range provide direct information on the generation, transfer, and confinement of high-energy electrons. In fact, the two earlier experiments revealed that hard X-ray imaging observations were very promis-

[1] Institute of Astronomy, University of Tokyo, Mitaka, Tokyo 181, Japan.
[2] Department of Physics, Faculty of Science, University of Tokyo, Bunkyo-ku, Tokyo 113, Japan.
[3] Institute of Space and Astronautical Science, Sagamihara, Kanagawa 229, Japan.
[4] National Astronomical Observatory, Mitaka, Tokyo 181, Japan.

* After the launch the name of SOLAR-A has been changed to YOHKOH.

Solar Physics **136:** 17–36, 1991.

ing, as expected. At the same time, the experiments should be regarded as preliminary ones; the two imagers had only one or two energy bands in the hard X-ray range, all below ~30 keV, and the angular and temporal resolutions were not sufficient. Thus, it is evident that an advanced hard X-ray imager will play a very important role to settle the puzzles of solar flares (e.g., Dennis, 1988). The Hard X-ray Telescope (HXT) for the SOLAR-A mission is such an instrument.

In the following, we will give an overview of HXT and its scientific objectives in Section 2. These objectives and the expected properties of the sources lead to X-ray optical design and the image synthesis principle (Section 3). Section 4 gives an outline of the HXT instrument. A few remarks will be made in Section 5 with regard to the performance of the flight instrument.

2. HXT Overview

The HXT is a Fourier-synthesis imager of 64 elements; each subcollimator measures a spatially-modulated incident photon count. A set of photon count data from the 64 subcollimators are telemetered to the ground and synthesized there into an image through, at least in principle, the Fourier transform.

Instrumentally HXT consists of three major sections (Figure 1).

The collimator (HXT-C) is the X-ray optics part of the instrument. Simply it is a metering tube (417 mm × 376 mm × 1400 mm) with X-ray grid plates at both ends. Each grid plate is an assembly of 64 subcollimator grids made of tungsten 0.5 mm thick. At the center of the X-ray optics is installed the aspect system (HXA) optics, which include lenses with appropriate filters on the front grid plate and fiducial marks on the rear plate, thus providing white-light images of the Sun which yield the axis direction information of the X-ray optics with respect to the solar disk. The HXT-C weighs ~13.5 kg.

The detector assembly (HXT-S; S denotes sensors) is a package of 64 detector modules (465 mm × 392 mm × 223 mm, weight ~17.1 kg); each module consists of a NaI(Tl) scintillation crystal (25 mm square) and a photomultiplier tube, with dynode bleeder string and pre-amplifier assembled as a unit. Eight high-voltage power supply units are attached to HXT-S. The HXT-S also has two one-dimensional CCD's at the center for detecting HXA visible-light signals.

The electronics unit (HXT-E) is 374 mm × 246 mm × 220 mm in size and ~10.8 kg in weight. It processes hard X-ray signals from HXT-S; first it converts pulse-height analogue signals into digital signals and then it counts the incident photon number after discriminating the photon energy into four energy bands. Here, signals from the individual subcollimators are processed separately and simultaneously. Finally HXT-E sends the photon count data to the data processor (DP; Ogawara *et al.*, 1991) of the spacecraft once every 0.5 s. The HXA signals are also digitized and processed in HXT-E. In addition HXT-E plays the role of power/mode controller of the whole HXT instrument.

The main characteristics of HXT are summarized and compared with its two pre-

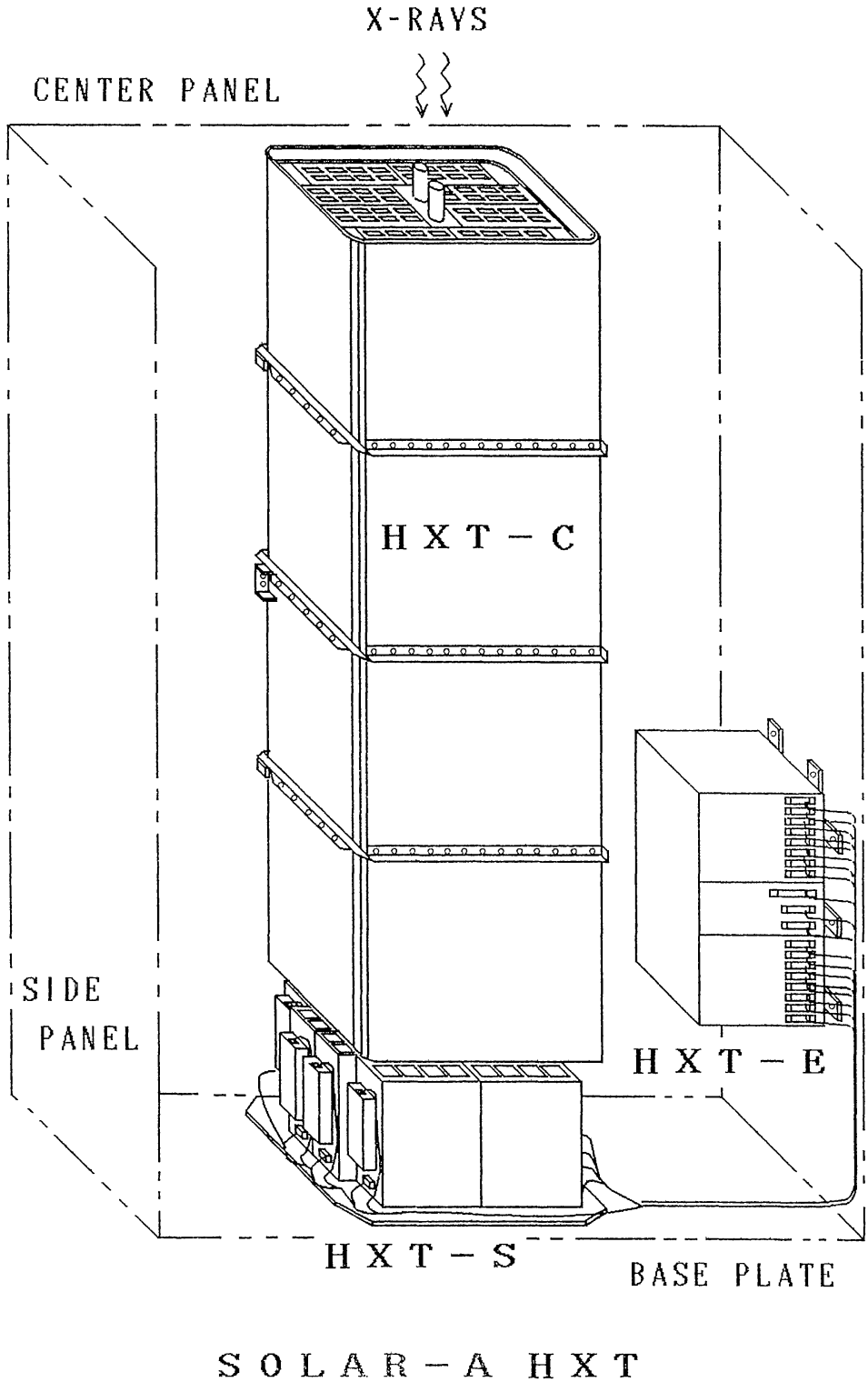

Fig. 1. Schematic drawing of the HXT instrument. HXT consists of three major sections: the collimator (HXT-C), the detector assembly (HXT-S), and the electronics unit (HXT-E). The aspect system (HXA) is installed along the central axis of HXT-C and HXT-S.

TABLE I

Main characteristics of HXT (comparison with its predecessors)

	HXT (SOLAR-A)	HINOTORI imager	HXIS (SMM)
Collimator type	Multi-el. bigrid MC	Rotating bigrid MC	Multi-el. IC
No. of elements	64 SC's	2 (orthogonal)	(F)304; (C)128
Size of elements	23 mm □	120 mm ∅	7.5 mm ∅
Image acquisition	2D Fourier synthesis	1D scans → 2D image	1 el./1 pixel
Angular resolution	~5″	~10″	8″ (32″)
Field of view	whole Sun	whole Sun	2′40″ (6′24″)
Synthesis aperture	2′06″	2′12″	2′40″ (6′24″)
Time resolution	0.5 s	~10 s	1.5–9 s
Energy bands (keV)	4 channels Ch. L: 15(19)–24 Ch. M1: 24–35 Ch. M2: 35–57 Ch. H: 57–100	1 channel 5(17)–40	6 channels 3.5–5.5–8.0 8.0–11.5–16 16–22–30
Detector	NaI(Tl) scint. (25 mm □ × 64)	NaI(Tl) scint. (120 mm ∅ × 2)	Gas prop. counter (7.5 mm ∅ × 900)
Effective area	~70 cm^2	~8 cm^2 × 2	0.07 cm^2 $pixel^{-1}$

Note: MC = modulation collimator; IC = imaging collimator; SC = subcollimator; 2D = two-dimensional; 1D = one-dimensional; (F) = fine field of view; (C) = coarse field of view.

decessors in Table I. As can be seen from the table, HXT has several advantages over its predecessors. These include:

- higher energy range to ~100 keV,
- higher sensitivity,
- improved angular and temporal resolutions,
- a wide field of view covering the whole Sun, and
- simultaneous observation with the Soft X-ray Telescope (SXT; Tsuneta *et al.*, 1991) on board the same mission.

With these advanced characteristics, HXT will make the first imaging observations in the $\gtrsim$ 30 keV hard X-ray range, collect many examples of hard X-ray flares, and help to answer the following specific questions about solar flares:

(1) Where are electrons accelerated in flaring magnetic flux loops: inside a highly-stressed single loop or at the interaction site of multiple loops?

(2) How does the acceleration process take place? Are electrons accelerated in a direction parallel to the magnetic lines of force or perpendicular? Or are electrons energized randomly? In what conditions does the process work?

(3) What causes the double-source structure of hard X-ray sources in impulsive (type B) flares? Do down-streaming electron beams exist and play an important role?

(4) Is there a different acceleration process operating in gradual hard (type C) flares from that of impulsive (type B) flares? What makes hard X-ray sources appear high in the corona?

(5) What determines the type of a flare? Is it a plasma parameter such as density or plasma β, or the magnetic field topology?

(6) Are electrons and ions accelerated simultaneously by a single process or separately? Are ions accelerated in a specific type of flare? If ions are accelerated in a different phase or step from electrons, what causes the second phase or step? (This topic will be pursued with simultaneous observations with the Gamma-Ray Spectrometer (GRS; Yoshimori *et al.*, 1991) on board the same mission.)

(7) How are the energized electrons confined in a magnetic flux loop or an arcade of loops? Does reacceleration of electrons take place?

(8) As a whole, what role does the acceleration of particles play in a flare? Is it a minor episode in a complicated flare process, or is it the main cause of subsequent thermal responses of the flaring solar atmosphere?

3. Design and Image Synthesis Principles

The HXT instrument is the world's first X-ray telescope that adopts the Fourier synthesis principle for taking images. This type of telescope was first discussed by Makishima *et al.* (1978) as multi-pitch modulation collimator (MPMC). Recently, in the course of design study for an advanced flare-oriented hard X-ray telescope, Prince *et al.* (1988) proposed a Fourier-transform telescope using position-sensitive detectors, each using one subcollimator and measuring one complex Fourier component.

The HXT is a Fourier-synthesis telescope with a novel design principle. Each subcollimator has a normal, non-position-sensitive detector and measures only one of a Fourier component pair. Here we use the term Fourier component for simplicity. Note that here and in the following the term does not have the usual sense – a coefficient in a series of trigonometric expansion of a function – but is generalized.

The design principle of HXT is based upon the fact that a single modulation collimator, with two identical grids having pitch (slit spacing) twice the slit width, gives a transmission function that is a repetitive triangular pattern. The function resembles the trigonometric (cosine or sine) function if we disregard the DC component involved. A brief explanation of the principle is given in Figure 2 and in what follows.

Let us represent the transmission function of one of a pair of subcollimators by

$$F_c(k\rho)\,; \qquad \rho = X\cos\theta + Y\sin\theta\,,$$

where k (= 1, 2, ...) denotes the wave number, $k\rho$ the modulation phase, θ the position angle of the grid pattern, and X and Y the spatial coordinates normalized to the fundamental (k = 1) period of repetition. In addition to this first subcollimator of the pair, there is a second whose position angle and pitch are the same as those of the first but whose relative slit positions are shifted by a quarter of the pitch. The transmission function of the second is then

$$F_s(k\rho) = F_c(k\rho - \pi/2)\,,$$

i.e., the pattern is the same as the first, but its phase is shifted by 90° from the first.

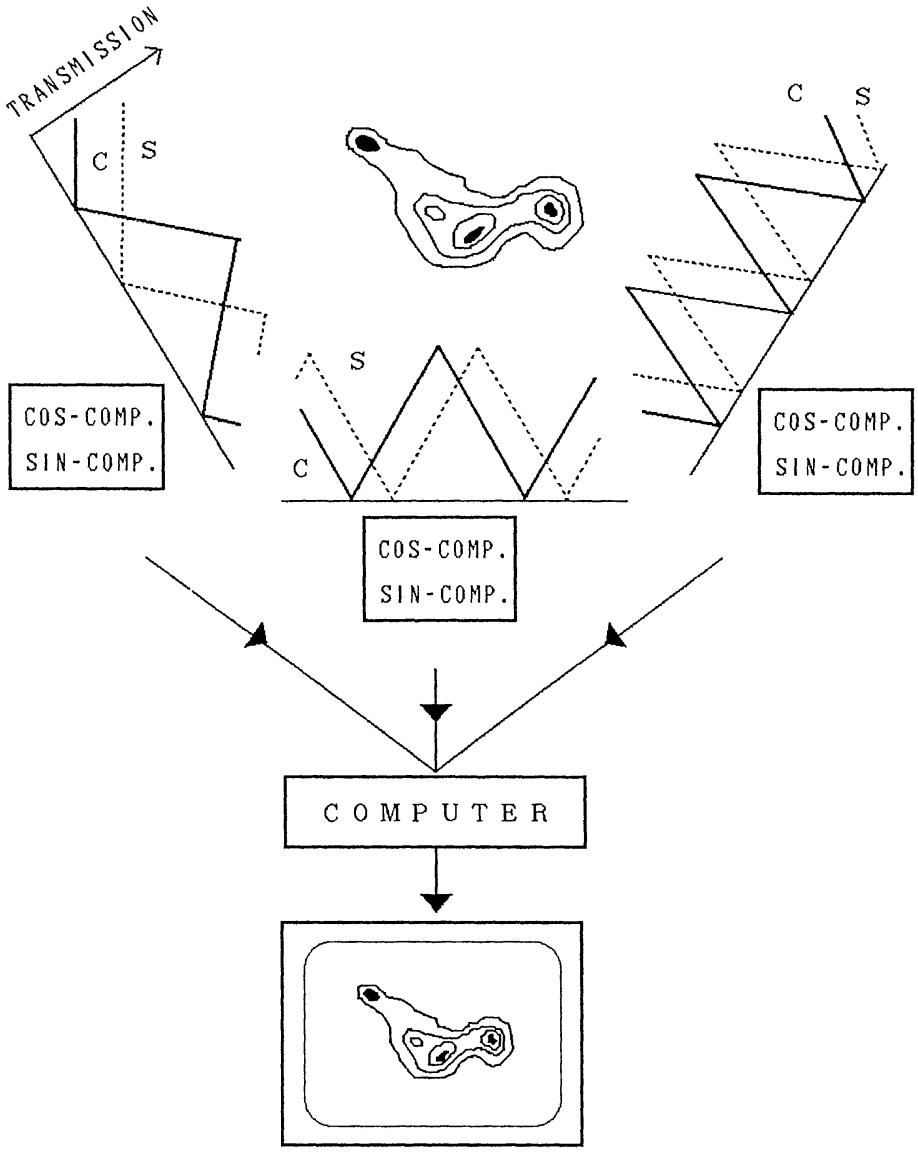

Fig. 2. Principle of Fourier synthesis for HXT. Pairs of photon counts taken through cosine and sine transmission patterns of subcollimators are synthesized into an image by inverse Fourier transform.

This relation is analogous to that between the cosine and sine functions. The subscript of F (C or S) is added to express this relation. Using the pair of subcollimators, we obtain two photon count data:

$$b_c(k, \theta) = A \int B(X, Y) F_c(k\rho)\, \mathrm{d}X\, \mathrm{d}Y,$$

$$b_s(k, \theta) = A \int B(X, Y) F_s(k\rho)\, \mathrm{d}X\, \mathrm{d}Y,$$

which represent one generalized complex Fourier component. Here $B(X, Y)$ is the X-ray brightness distribution to be imaged and A is an effective area of the subcollimator/detector system.

If the data actually represented a usual complex Fourier component, and also if measurements were made at a sufficient number of (k, θ)-points, $B(X, Y)$ could be calculated from an inverse Fourier transform. In HXT as in other applications, however, the two conditions are not fully satisfied. In the case of super-synthesis radio telescopes, radio astronomers have developed an image synthesis procedure called CLEAN (Högbom, 1974) for the reconstruction of an image from an incomplete set of measurements. Even the first condition is not a vital one; radio and X-ray astronomers have introduced the maximum entropy method (MEM) for reconstructing an image, where no specific requirement is made on the transmission patterns (e.g., Frieden, 1972; Gull and Daniell, 1978; Willingale, 1981). Thus the sophisticated problems such as the orthogonality and completeness of a system of functions in the mathematical sense are not required to be directly related to the HXT image synthesis problem of ours. Rather our problem is a more practical one.

The following describes our practical approach to image synthesis, using simulated sources and realistic HXT response properties. First we wrote computer programs to simulate the observations and to perform image syntheses. For the image synthesis step, using the analogy of HXT with radio telescopes of Fourier-synthesis type and also benefiting from our previous HINOTORI observations (Tsuneta, 1984; Kosugi and Tsuneta, 1983), we adopted two methods in parallel: one is MEM and the other modified CLEAN. The original CLEAN technique makes use of the Fourier transform to synthesize dirty maps and this transform cannot be applied to our case, so that this part was replaced by a newly-developed procedure.

Next we made numerous computer simulations for a wide variety of model brightness distributions and at different intensity levels. The purposes of the simulations are threefold:

(1) to confirm that the design principle of HXT is correct and that the above-mentioned image synthesis methods work well;

(2) to find the minimum number of subcollimators and also the optimum arrangement of them on the (k, θ)-plane; and

(3) to know the effect of observation errors, namely the effective area error and the phase error, on the quality of synthesized images.

Before making the simulations, a few *a priori* assumptions and restrictions were introduced in the HXT design study. An assumption was that the angular extent of the hard X-ray flare is less than ~ 2 arc min; this determines the fundamental period of repetition or the 'synthesis aperture' ($= 2'06''$). The SMM and HINOTORI results suggest that this assumption is not unreasonable. We chose the highest wave number, $k_{\max}$, to be 8 (in units of the fundamental spatial frequency). This choice is a compromise with the difficulty of fabricating fine grids. Finally we used a symmetrical polar diagram (k, θ), not a rectangular grid for arranging the subcollimators on the (u, v)-plane. This is because an arrangement of subcollimators at regular lattice points on the (u, v)-plane produces on the image plane a repetitive pattern with the fundamental period (so-called grating response) resulting in ambiguity of the flare position.

From the simulations we confirmed the feasibility of partial (u, v)-plane coverage, at

least as far as a sufficient number of, say, more than ~50, complex Fourier components are available. As the number of subcollimators is reduced, the quality of the synthesized images becomes gradually worse. At the same time, the synthesized images from a set of Fourier elements alone tend to deteriorate for relatively extended sources. We found that this tendency can be overcome by replacing the Fourier elements at low wave numbers by what we call 'fanbeam elements' (cf. Figure 3). On the other hand, replacement of Fourier elements at high wave numbers by fanbeam elements results in reduced angular resolution.

Considering all these results together with construction and maintenance problems, we have determined the number of subcollimators to be 64 and chosen as the optimum design the subcollimator arrangement on the (k, θ)-plane as shown in Figure 3.

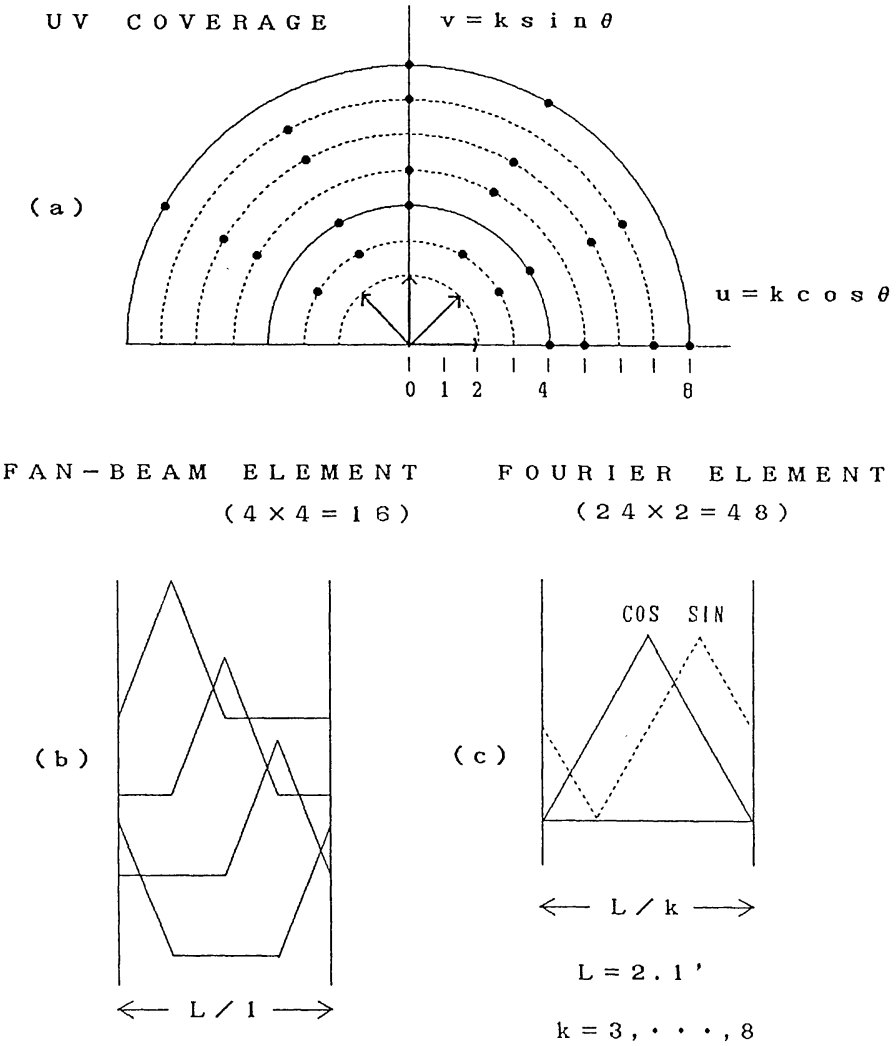

Fig. 3. (a) Arrangement of subcollimators in Fourier-transform space, the (u, v)-plane in which u and v represent the spatial wave numbers of the modulation pattern. Each dot denotes the position at which one pair of Fourier-element subcollimators provides angular information. The fanbeam elements provide information along the arrows near the origin of the (u, v)-plane. The wave number k is given in units of the fundamental repetition period, i.e., 2.1 arc min. (b) The modulation patterns for a set of fanbeam elements. (c) Same as (b) for a Fourier-element pair.

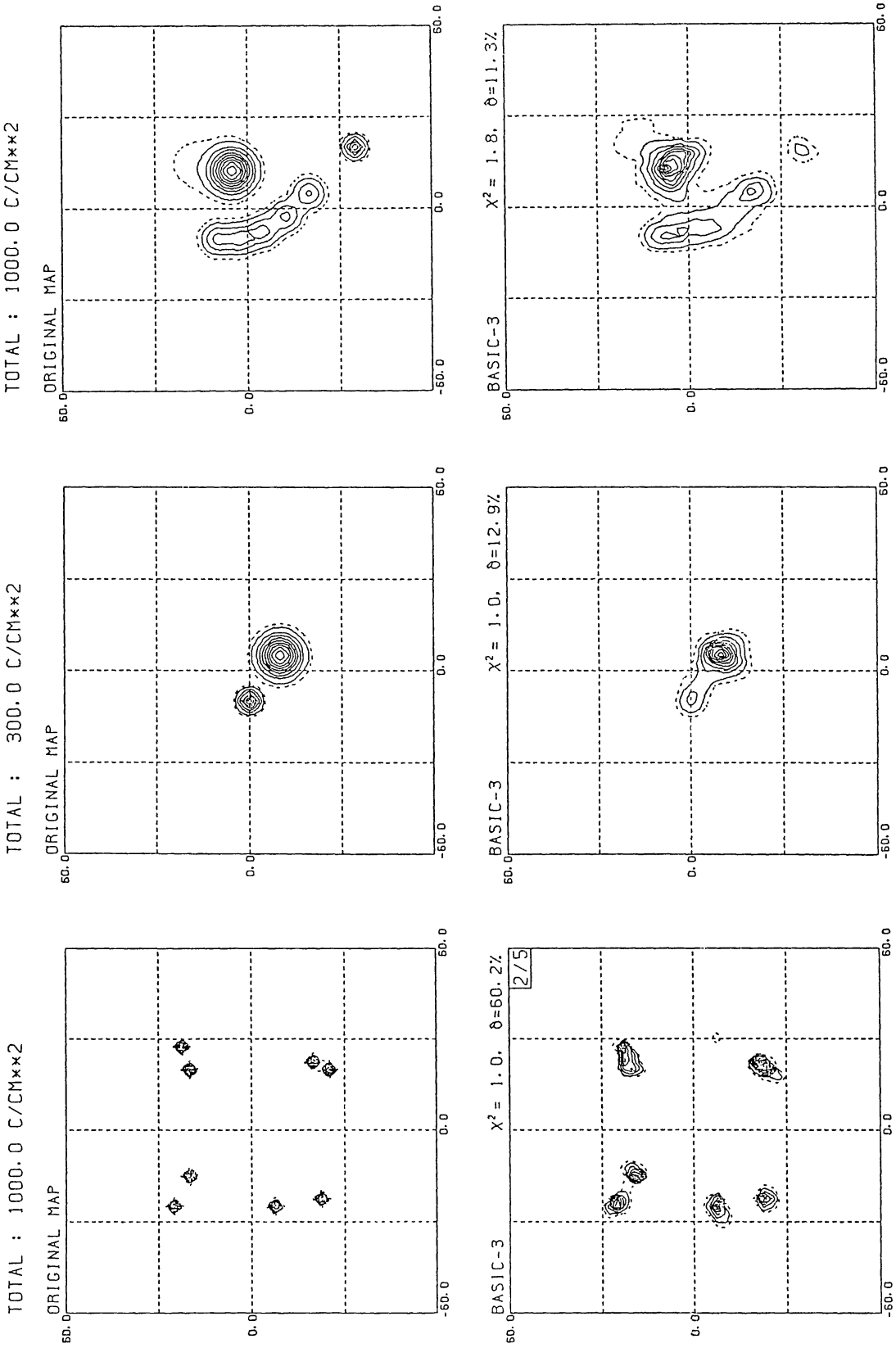

Fig. 4. Examples of image-synthesis simulations by MEM for the actual HXT design. Restored maps (*bottom*) are compared with the corresponding original maps (*top*) for scattered compact sources (a), double sources (b), and diffuse sources (c). Contour levels are 10% steps (solid lines) and 5% (dashed lines) of the peak. Each box is ~2 × 2′. The incident X-ray fluence is given at the top. The separations between the adjacent sources in (a) are 6″, 8″, 11″, and 15″. The phase error of 1.0″ (r.m.s.) of the 64 transmission functions is incorporated in addition to the Poisson noise in (c).

Examples of synthesized images obtained from the simulations corresponding to the actual design of HXT are shown in Figure 4. The angular resolution experimentally determined from simulations is ~ 5 arc sec.

With regard to the observation errors, we obtained the following results:

(1) The effective area and phase errors do not severely deteriorate the image quality *if* they are correctly evaluated, since they can be removed in the image synthesis procedure.

(2) The synthesized images become quite unstable, when:

– the effective areas of the 64 subcollimators are not evaluated with an accuracy of less than 5% in the r.m.s. sense, or

– the peak positions of the 64 transmission functions are not evaluated with an accuracy of less than 1 arc sec in the r.m.s. sense.

It is to be remarked that the effective area errors are not only related to the subcollimator optics but also to the detector/electronics system of HXT, since the photon count is very sensitive to the energy discrimination levels. Considering the steepness of the flare hard X-ray spectrum (power-law spectrum with the index around $\gamma \approx 4$), the $\sim 5\%$ accuracy in effective area corresponds to $\sim 1\%$ accuracy requirement on the gain of the pulse-height analysis. The peak position error criterion may be slightly relaxed for subcollimators at low wave numbers.

4. The Instrument

From the viewpoint of structure, HXT is divided into three major sections, i.e., the collimator (HXT-C), the detector assembly (HXT-S), and the electronics unit (HXT-E). Functionally it is divided into the X-ray optics part, the X-ray detection/signal processing part, the aspect system (HXA) part, and the power/mode control part. The spacecraft data processor (DP) also plays a role in editing HXT data.

Thus in the following, first we will give an outline of HXT-C, HXT-S, and HXT-E in Sections 4.1 through 4.3, respectively, with concentrated attention to the X-ray detection/signal processing part. The HXA-related items will be described separately in Section 4.4 and the data handling in DP in Section 4.5. The power/mode control of HXT will be mentioned where it is necessary.

4.1. Collimator (HXT-C)

The roles of HXT-C are the X-ray optics, which provide the 64 independent transmission (modulation) patterns necessary for synthesizing images, and the HXA optics. The two sets of optics require high standards of structural stability to permit coalignment between the individual subcollimators and also between the X-ray and HXA optics systems; note that, if absolute alignment of the order of 1 arc sec is required, a relative shift of one grid with respect to the others smaller than ~ 10 μm should be held. Thus the whole system of HXT-C (except for some minor portions corresponding to two visible-light paths for HXA) is covered by a thermal shield to maintain as homogeneous and stable a temperature as possible. The HXT-C is thermally completely passive.

4.1.1. *Metering Tube*

The metering tube of HXT is a box 1400 mm long and sustains two grid assemblies each 402 mm × 362 mm wide and ~3 kg in weight at both ends by face plates. Because of weight and stiffness requirements, the tube is made of CFRP (carbon-fiber reinforced plastic; $\rho \sim 1.7\ \mathrm{g\ cm^{-3}}$) with twelve carbon-fiber sheets stratified quasi-isotropically for minimizing the coefficient of thermal expansion ($\alpha < 1 \times 10^{-6}\ \mathrm{deg^{-1}}$ is achieved). The CFRP box is ~1.3 mm thick at the side plates and ~2.1 mm thick at the face plates, with three stiffeners encircling the side plates. The stiffeners are also used as attachment points to the spacecraft body (cf. Figure 1). The metering tube itself weighs ~8.0 kg.

Mechanically the tube is very resistive against deforming forces. Since any small lateral shift of the rear face plate with respect to the front one can be calibrated by HXA, the most damaging deformation mode for the X-ray optics is a twist between the front and rear plates. The tube stiffness against a twisting torque T is given by

$$\theta\,(\mathrm{arc\ min}) = 0.025T\,(\mathrm{kg\ m})\,.$$

The metering tube is thus extremely stiff, stiffer than the spacecraft center panel to which HXT-C is attached; however, it is still possible that thermal expansion or mechanical deflection of the center panel would deform the metering tube at a certain level. Accordingly a special attachment has been devised to avoid such an effect.

4.1.2. *Grid Assemblies*

The two grid assemblies carry the tungsten grids for the 64 X-ray subcollimators. The aspect lenses with filters are at the center of the front grid assembly, and the fiducial marks at the corresponding position on the rear. The two grid assemblies are fastened by screws to the CFRP face plates.

Each grid assembly consists of a base plate, four fanbeam element units, and six Fourier element units (Figure 5(a)). The base plate is a single molybdenum plate 1.5 mm thick and holds both the X-ray elements and the aspect optics. The plate has 64 square holes (with rounded corners) for the X-ray optics. Each hole has a dimension of 37 mm (front) and 23 mm (rear). The size of the rear hole determines the aperture (effective area) of each subcollimator, and the front hole is larger than the rear one to give full aperture efficiency at any point on the Sun.

Each of the fanbeam element units is a 0.5-mm thick tungsten plate with four fanbeam grids of one position angle, and is set at a corner of the base plate. The grids are fabricated by the electric discharge method. On the other hand, the six Fourier element units, each with eight Fourier grids of one position angle, are the stack of ten tungsten foils, each 50 μm thick, with a molybdenum covering plate 0.5 mm thick. The grids are fabricated by the photo-etching processing. The grid parameters are summarized in Table II.

Figure 5(a) schematically shows the geometrical arrangement of the 64 subcollimators. This diagram shows the slit directions, wave numbers, and the locations of the cosine and sine pairs. The rules for the layout are:

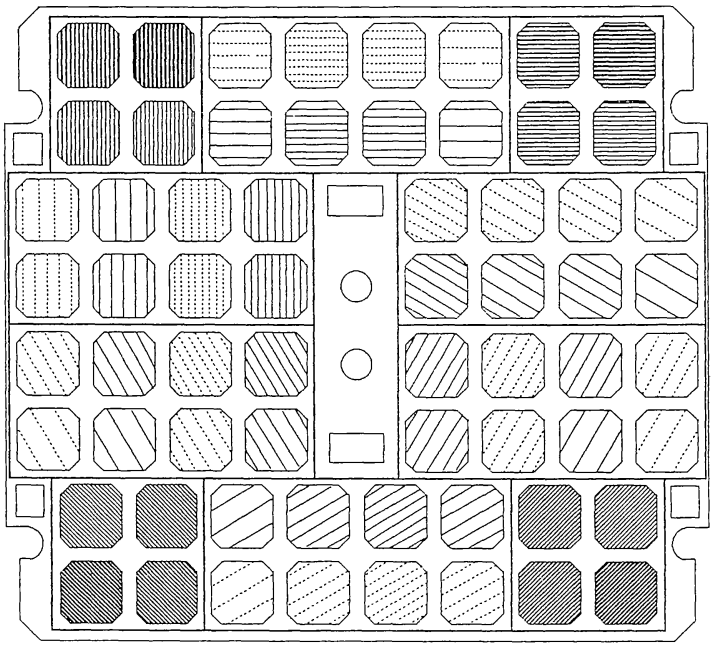

Fig. 5a. Arrangement of the 64 subcollimators on the grid assemblies (top view). The slit directions of the individual grids are represented by the hatching. The cosine and sine Fourier element pairs are shown by solid and broken hatching lines, respectively, with the number of lines denoting the wave numbers.

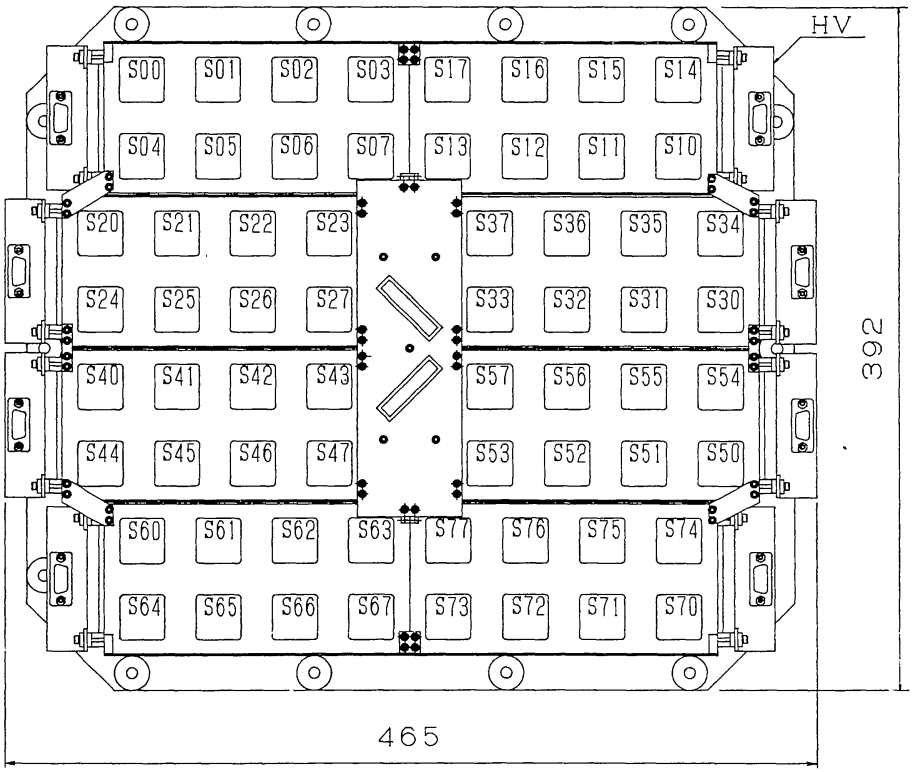

Fig. 5b. Top view of the detector assembly (HXT-S). The numbered (in octal) squares represent the 64 scintillation counters, grouped in units of 8 modules as shown. At the left- and right-hand sides, the sketch shows the 8 high-voltage supplies, one for each detector unit. The inclined oblong boxes represent the one-dimensional CCD arrays of the HXT aspect system.

TABLE II

Grid main parameters

	Fanbeam elements	Fourier elements
Number of elements	16	48
Mosaic structure	4 el. × 4	8 el. × 6
Position angles	0, 45, 90, 135 deg	0, 30, 60, 90, 120, 150 deg
Number of phases	4 (90° step)	2 (cosine and sine)
Wave numbers	$k = 1, 2$	$k = 3, 4, 5, 6, 7, 8$
Pitch (arc sec)	126	42.0, 31.5, 25.2, 21.0, 18.0, 15.8
Slit width (μm)	210	140, 105, 84, 70, 60, 60
Wire width (μm)	630	140, 105, 84, 70, 60, 45
Material	0.5 mm thick tungsten	0.05 mm thick tungsten foil × 10
Process method	electric discharge	photo etching

(i) The elements of the same position angle are put together in the same unit. This is to make it easy to synthesize one-dimensional images with less danger of phase errors between the same position-angle elements.

(ii) The cosine–sine pair are located adjacent to each other, because to keep the phase difference at exactly 90° is of vital importance.

(iii) Elements with higher wave numbers are concentrated toward the central portions of the assemblies, and the slit directions are selected to be as nearly tangential as possible. This is for reducing a bad effect in case the metering tube happens to twist.

In order to assemble the X-ray optics with very high accuracy, each component has an appropriate number of knockpin holes which ensure a positional accuracy of ~ 5 μm. Also the grid assemblies have six additional grid patterns (two at the center near the aspect optics and four on the fanbeam element units) together with through holes which transmit visible light. They are used for the purpose of coalignment between the front and rear assemblies.

4.2. Detector Assembly (HXT-S)

As shown in Figure 5(b), the detector assembly is composed of 64 identical detector modules, eight high-voltage power supplies (each for eight detector modules), and two one-dimensional CCD arrays for the aspect optics.

4.2.1. *Detector Modules*

A detector module consists mainly of a NaI(Tl) scintillation crystal and a photo-multiplier tube; each module has a high-voltage bleeder string and pre-amplifier in its housing (Figure 6). Eight detector modules are packed together to form a detector unit in a magnesium frame, and eight detector units are tied together to form the detector assembly. The detector part is thermally shielded from the high-voltage power supplies, the main heat sources. The high heat conductivity helps to keep the temperature inside the detector assembly homogeneous.

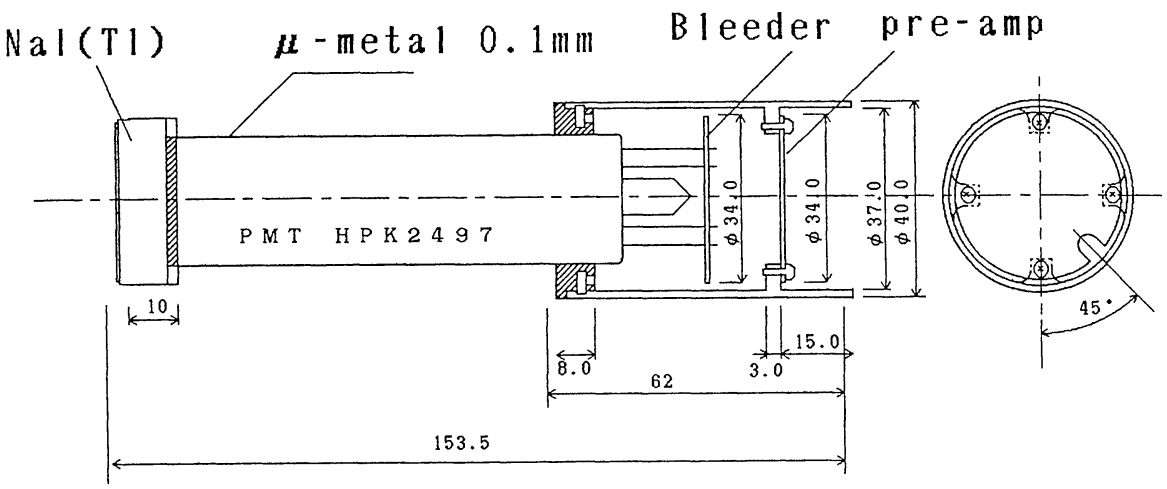

Fig. 6. Schematic drawing of a detector module.

The crystal has a slightly larger dimension (25 mm) than the grid aperture. It is 5 mm thick, which determines the X-ray detection efficiency at high energies. The crystal is surrounded by an aluminum case. The case, 0.8 mm ($\pm$ 0.01 mm) thick at the front of the crystal, plays the role of an X-ray filter to avoid pulse pile-up due to the flare soft X-rays. In addition to the aluminum filter, X-rays pass through the two CFRP face plates each 2.1 mm thick. Figure 7 shows the spectral response of HXT. (Also is given in this figure the absorption efficiency or the stopping power of the 0.5-mm tungsten plate.)

The photomultiplier tube (HPK 2497 from the Hamamatsu Photonics Co.) is of an anti-vibration type, and is magnetically shielded by μ-metal to suppress gain variation.

The energy resolution (FWHM) of a typical module is given experimentally as

$$\Delta E/E \sim 1.3E^{-1/2} \quad (E \text{ in keV}),$$

a normal value for a NaI(Tl) crystal.

For calibrating the pulse-height gain, a calibration source is attached for each module at the center of the aluminum case front cover. The source is a radioisotope ^{241}Am whose line emission at 59.5 keV is used as a reference point of the pulse-height gain. Since the source is physically small (4 mm^2; $\sim 0.6\%$ of the aperture) and gives only a few to several counts s^{-1} per detector, it does not interfere with flare observations. (A special output mode of HXT data exists for calibration data, see Section 4.3.)

The time constant of the charge amplifier is ~ 10 μs so that each detector can measure incident photon counts up to a few times 10^4 cts s^{-1} without being strongly bothered by the pulse pile-up problem. This limit is large compared to the largest flare yield expected to be $\sim 10^4$ cts s^{-1}.

4.2.2. *High-Voltage Power Supply Units*

One DC-DC converter supplies high voltage to the eight modules in one detector unit. The output voltage of each converter can be chosen from eight levels by a command from the ground. The eight levels are initially set to be between ~ 800 V and ~ 1050 V

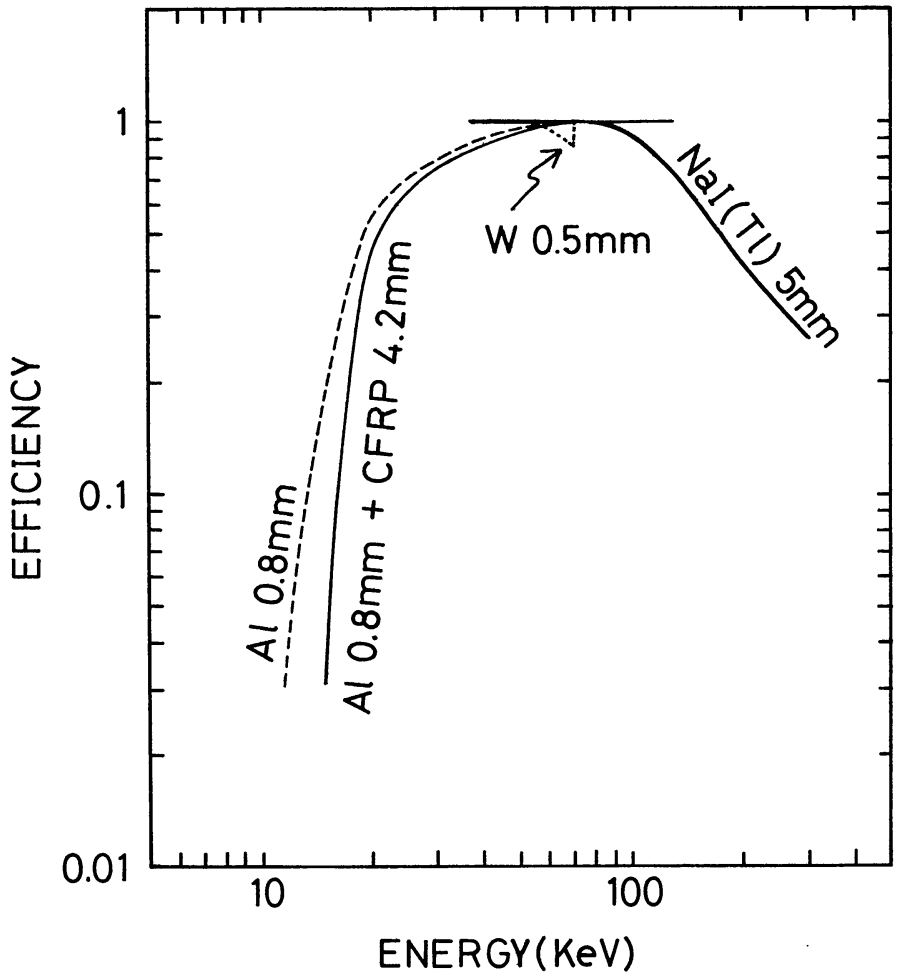

Fig. 7. Spectral responses of HXT-S and HXT-C. The detection efficiency against X-ray photon energy of the NaI(Tl) scintillation crystal (5 mm thick) is shown by the thick line; the transmission efficiencies of the Al filter (0.8 mm thick) alone and plus the two CFRP face plates (each 2.1 mm thick) by dashed and thin lines, respectively; and the absorption efficiency or the stopping power of the tungsten grids (0.5 mm thick) by dotted line.

with a step of ~ 35 V. This enables us to adjust the pulse-height gain of the eight modules simultaneously by a step of $\sim 20\%$ (coarse gain adjustment).

The high-voltage output can be reduced to nearly zero without turning off the control circuit of the supply. This function is used when the spacecraft enters the radiation belt, where photomultiplier tubes could be damaged if high voltage continued to be supplied; leaving the control circuit on increases the stability of the output. This function is also used during satellite night when all the HXT analogue electronics part turns off to reduce the power consumption.

4.3. Hard X-ray signal processing in the electronics unit (HXT-E)

The block diagram of the X-ray signal processes is shown in Figure 8. Each of the analogue signals sent from the 64 modules is first gain-adjusted by an operational amplifier. Here the level of the gain is chosen by a command from 64 levels with a step

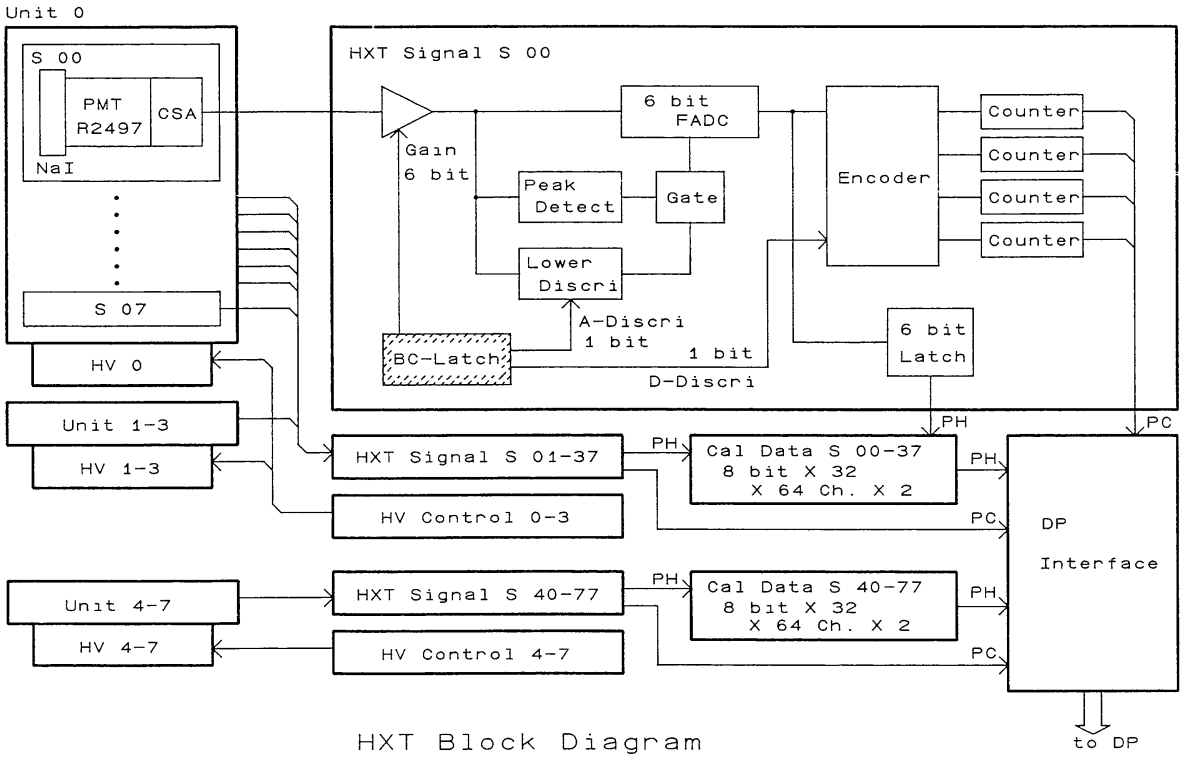

Fig. 8. Block diagram of the X-ray signal processing electronics (see text).

of $\sim 1\%$ (fine gain adjustment). Then, in the peak detection circuit, pulses contained in the signal are detected one by one and digitized by a 6-bit flash A/D converter (RCA CA3306D) whenever the pulse height exceeds the analogue discrimination level (selectable from two levels corresponding to ~ 15 and ~ 19 keV, both slightly lower than the corresponding digital discrimination levels; see below). The 6-bit value is nominally related to the incident photon energy as

$$\text{energy (keV)} = (1.35 \times \text{value}) + 13.6 \, .$$

Up to this point the 64 modules are independent, each with its own circuit. Further signal processing depends on the operation mode of HXT, observation or calibration.

4.3.1. *Observation Mode* (*Pulse Count Mode*)

When observing the Sun, each digital data value is sent to an encoder for binning into one of the four counters as detailed in Table III with the nominal photon energy range. The digital value that corresponds to the lower limit of channel 'L' (digital discrimination level) is selectable between values of 1 or 4. Pulses with values lower than this number are not counted in any of the channels.

All photon count data from the 256 ($= 4 \times 64$) counters are sent to the spacecraft data processor every 0.5 s simultaneously. Each counter is 12 bits so that the maximum count is 4095. It can be used cyclically when the photon count exceeds this number, although such big flares rarely occur.

TABLE III

Four PC channels in the observation mode

Channel	Digital data value	Energy range (nominal)
L	1(4) – 7	15.0(19.0)–24.4 keV
M1	8–15	24.4–35.2
M2	16–31	35.2–56.8
H	32–63	56.8–100.0

4.3.2. *Calibration Mode* (*Pulse Height Mode*)

This mode starts and ends when so commanded from the ground. In this mode each digital value is sent together with the detector module number to the counter memory, where the photon count is binned in 64 channels directly corresponding to the digital pulse heights. The memory consists of two buffers, each of which is 4096 (= 64 × 64)-channel, 8-bit counters, for ensuring data accumulation during the data transfer. These pulse height data are sent to the data processor every 8 s.

Since this mode is used for calibrating the pulse-height gain of the individual modules, it is turned on when the background noise is expected to be the smallest during spacecraft night. In good conditions and with an integration time of ~ 1000 s, we can measure the peak position of the 59.5 keV emission line to an accuracy less than a few percent. Actually the gain calibration measurement will be repeated till a uniformity of the gain to $\sim 1\%$ between the 64 modules is attained. Thanks to the stability of the modules and circuits we expect readjustment to be necessary less than once per month.

4.4. Aspect system (HXA)

The scientific return of HXT strongly depends on whether the positions of hard X-ray sources can be determined with respect to the soft X-ray and visible-light features observed with the Soft X-ray Telescope and ground-based instruments. This is achieved by the aspect system (HXA) with approximately 1 or 2 arc sec accuracy. Although the spacecraft has an attitude control system equipped with aspect sensors (a Sun sensor and a star tracker) and an inertial reference unit which can provide the aspect of the spacecraft with less than 1 arc sec accuracy and a sufficient time resolution, none of them can be coaligned with the X-ray optics of HXT accurately enough for this purpose. The HXA optics, mounted at the center of the two grid assemblies, provide the precise information necessary.

The HXA optics consist of two identical systems. Each is composed of an achromatic, doublet imaging lens 10 mm in diameter with filters on the front grid assembly, a set of fiducial marks located on the rear grid assembly, and a one-dimensional CCD which is placed at the top of HXT-S and measures the white-light brightness distribution of the Sun. The lens center and fiducial marks determine the HXA optical axis, which is referred to as the X-ray 'axis' by metrology. The two CCD's are set to the orthogonal directions to each other.

In HXT-E the CCD video signals are digitized and processed in two complementary ways in parallel. One is that the addresses of pixels whose video signals intersect the discrimination level (selectable from four levels) are sent to the data processor one every second. The other is the output of the complete brightness distributions at a slower rate of once every 64 s (high telemetry bit rate case).

4.5. Onboard data handling in the data processor (DP)

The spacecraft data processor (Ogawara *et al.*, 1991) receives HXT data and edits them together with other scientific and auxiliary data into a telemetry format according to the observing mode (quiet, flare, night, and BCS-out mode) and the telemetry bit rate (32, 4, or 1 kbps). Here we briefly summarize HXT-related items.

4.5.1. *Pre-storage of X-Ray Data for 4 s*

The HXT data have no allocation of telemetry words in quiet mode except for channel 'L'. This is not unreasonable because almost no hard X-rays are emitted from outside flaring regions. The problem is, however, that the flare flag can only be set after a flare commences, so that a few seconds elapse before the automatic mode change. In order to avoid loss of initial data of a flare, all the X-ray data from HXT are kept in a buffer for 4 s before sent to the subsequent processing, regardless of mode or the telemetry bit rate.

4.5.2. *Time Resolution and Sampling*

In flare mode the data processor transmits four-channel HXT data at 0.5 s resolution (high bit rate) or at 4 s resolution after integration (medium bit rate). In addition to this, the channel 'L' data are separately transmitted at 2 s (high bit rate) or 16 s (medium bit rate) resolution as a backup for all observing modes except during spacecraft night when the HXT analogue electronics turn off. Although this backup output is mainly for house-keeping purposes, it also provides scientific data for preflare or postflare hard X-ray images.

4.5.3. *Data Compression*

Each 12-bit pulse count data word is reduced (after any summing of individual 0.5 s data) to an 8-bit number according to the following function:

$$\begin{aligned} m &= n && (n = 0\text{–}15)\,, \\ m &= \mathrm{int}(4 \times \sqrt{n}) && (n = 16\text{–}4080)\,, \\ m &= 255 && (n = 4081\text{–}4095)\,, \end{aligned}$$

where $\mathrm{int}(x)$ represents the truncated integer value of x. This mapping ensures that digital error due to the bit reduction is always smaller than the Poisson noise statistical error by a factor of two, i.e.,

$$\Delta n' = [(m + 1)^2 - m^2]/16 \sim m/8 \sim \sqrt{n}/2\,.$$

Because of this, the n' values estimated from 8-bit m's have almost the same standard deviations as the original n values.

5. Final Remarks

As is summarized in Table I, the design characteristics of HXT greatly improve on those of its two predecessors. Because it is a Fourier-synthesis telescope, it achieves both high sensitivity and wide field of view. The modulation of X-rays up to ~ 100 keV becomes possible owing to the precise fabrication of tungsten grids by the electric discharge and photo-etching methods. The HXT owes its improvement over the HINOTORI hard X-ray imager not only to the precision of its fine grids but also the increased length of the metering tube. Nevertheless, almost all these improvements are simply elements of the design and do not directly determine the practical performance of HXT as an imager. Since HXT is a telescope with 64 independent subcollimators, what determines the image quality of HXT is very complicated. The most important factors are:

– preciseness of the individual grids,

– coalignment between the 64 subcollimators within ~ 1 arc sec accuracy,

– evaluation of the individual patterns as functions of X-ray energy as accurately as possible, and

– calibration and adjustment of the individual pulse-height gain with accuracy of $\sim 1\%$.

None of these four have been achieved easily. In addition, for hard X-ray images to be successfully compared with images taken with other telescopes, coalignment between the X-ray and HXA optics within a few arc sec is highly desirable.

We have carefully examined the following points during assembling since all the components of HXT were completed in the summer of 1990:

(1) The X-ray grids, examined with microscopes, are well fabricated; individual slits in a grid are cut with accuracy less than 10 μm in position and the average slit pitch differs from the design value by less than 1 μm.

(2) We have examined the coalignment among the 64 subcollimators, using both optical and X-ray methods with the separation between the front and rear grid assemblies reduced, and obtained accurate enough phase-error data for the 64 subcollimators.

(3) The X-ray modulation patterns for the individual subcollimators have been evaluated at photon energies below ~ 40 keV. (No X-ray beams are available at higher photon energies.)

(4) We have checked that the pulse-height gain of the individual detector modules can be adjusted to an accuracy of $\sim 1\%$.

(5) Regarding the coalignment between the X-ray and HXA optics, we have measured the misalignment due to the prism effect, etc., of the HXA optics with an accuracy of a few arc sec.

Calibration measurements will be continuously executed with higher accuracy until the launch.

Acknowledgements

We acknowledge Professors Minoru Oda, Yasuo Tanaka, and the late Prof. Katsuo Tanaka, without whose efforts the SOLAR-A project would not have existed. Dr Keizo Kai, Principal Investigator of HXT and one of the authors of this paper, passed away on 11 March, 1991, one day after this paper was submitted to *Solar Physics*. The rest of the authors wish to express their deep sorrow as well as their will to successfully accomplish this project. The HXT project is a joint effort between the Institute of Space and Astronautical Science, the National Astronomical Observatory, and the University of Tokyo (including both the Department of Physics and the Institute of Astronomy). This work is partially supported by the Scientific Research Fund of the Japanese Ministry of Education, Science and Culture under Grant Nos. 01540214 and 02452011.

References

Dennis, B. R.: 1988, *Solar Phys.* **118**, 49.
Frieden, B. R.: 1972, *J. Opt. Soc. Am.* **62**, 511.
Gull, S. F. and Daniell, G. J.: 1978, *Nature* **272**, 686.
Högbom, J. A.: 1974, *Astron. Astrophys. Suppl.* **15**, 417.
Kosugi, T. and Tsuneta, S.: 1983, *Solar Phys.* **86**, 333.
Makishima, K.: 1982, in Y. Tanaka *et al.* (eds.), *Proc. Hinotori Symp. on Solar Flares*, ISAS, p. 120.
Makishima, K., Miyamoto, S., Murakami, T., Nishimura, J., Oda, M., Ogawara, Y., and Tawara, Y.: 1978, in K. van der Hucht and G. S. Vaiana (eds.), *New Instrumentation for Space Astronomy*, Pergamon Press, New York, p. 277.
Ogawara, Y., Takano, T., Kato, T., Kosugi, T., Tsuneta, S., Watanabe, T., Kondo, I., and Uchida, Y.: 1991, *Solar Phys.* **136**, 1 (this issue).
Prince, T. A., Hurford, G. J., Hudson, H. S., and Crannell, C. J.: 1988, *Solar Phys.* **118**, 269.
Tsuneta, S.: 1984, *Ann. Tokyo Astron. Obs., 2nd Series* **20**, 1.
Tsuneta, S., Acton, L., Bruner, M., Lemen, J., Brown, W., Caravalho, R., Catura, R., Freeland, S., Jurchevich, B., Morrison, M., Ogawara, Y., Hirayama, T., and Owens, J.: 1991, *Solar Phys.* **136**, 37 (this issue).
Van Beek, H., Hoyng, P., Lafleur, B., and Simnett, G. M.: 1980, *Solar Phys.* **65**, 39.
Willingale, R.: 1981, *Monthly Notices Roy. Astron. Soc.* **194**, 359.
Yoshimori, M., Okudaira, K., Hirasima, Y., Igarashi, T., Akasaka, M., Takai, Y., Morimoto, K., Watanabe, T., Ohki, K., Nishimura, J., Yamagami, T., Ogawara, Y., and Kondo, I.: 1991, *Solar Phys.* **136**, 61 (this issue).